Available online at www.sciencedirect.com
ScienceDirect
Acta Materialia 54 (2006) 5281–5291
Acta MATERIALIA
www.actamat-journals.com

Plastic strain-induced grain refinement at the nanometer scale in copper

K. Wang [a], N.R. Tao [a,*], G. Liu [a], J. Lu [b], K. Lu [a]

[a] *Shenyang National Laboratory for Materials Science, Institute of Metal Research, Chinese Academy of Sciences, Shenyang 110016, China*
[b] *Department of Mechanical Engineering, Hong Kong Polytechnic University, Hong Kong, China*

Received 24 April 2006; accepted 2 July 2006
Available online 27 September 2006

Abstract

Microstructural evolution and grain refinement in pure Cu subjected to surface mechanical attrition treatment (SMAT) were investigated by means of systematic transmission electron microscope observations. Two different mechanisms for plastic strain-induced grain refinement in Cu were identified, corresponding to different levels of strain rate. In the subsurface layer of the SMAT Cu samples with low strain rates, grains are refined via formation of dislocation cells (DCs), transformation of DC walls into sub-boundaries with small misorientations, and evolution of sub-boundaries into highly misoriented grain boundaries. The minimum size of refined grains via this process is about 100 nm. In the top surface layer (thickness <25 μm) with a high strain rate, the grain refinement includes: (i) formation of high-density, nanometer-thick twins dividing the original coarse grains into twin–matrix (T–M) lamellae; (ii) development of dislocation walls that further subdivide the T–M lamellae into equiaxed nano-sized blocks; (iii) evolution of these preferentially oriented blocks into randomly oriented nanosized grains. The minimum size of such refined grains is about 10 nm. The present study demonstrates the critical role of strain rate on the plastic strain-induced grain refinement processes and on the minimum grain size obtainable via plastic deformation.

Keywords: Grain refinement; Copper; Plastic deformation; Mechanical twinning; Strain rate

1. Introduction

Grain refinement induced by plastic strain in metals is a well-known phenomenon. Various techniques based on plastic strain have been developed for substantially refining grains in metals and alloys in order to enhance their properties. For example, cold-rolling [1,2] and different severe plastic deformation (SPD) approaches (e.g., equal channel angular pressing (ECAP) and high pressure torsion (HPT)) [3–6] have been used for synthesizing ultrafine-grained materials (with grain sizes in the submicrometer regime) the mechanical strength of which is remarkably elevated. Understanding of the underlying mechanism of strain-induced grain refinement is crucial not only from a theoretical point of view, but for technological development of advanced plastic deformation techniques for engineering applications.

The mechanism of grain refinement based on plastic straining has been extensively investigated in numerous materials [7–11]. It has been well documented that for those materials with medium or high stacking fault energies (SFEs), such as Fe, Cu and Al, coarse grains are refined upon continued straining by various dislocation activities. For example, strain-induced grain refinement in Cu, the most frequently studied sample on this topic in recent years, involves the following processes [11]: (i) manipulation of lattice dislocations; (ii) formation of dislocation cells and/or dense dislocation walls that subdivide the original coarse grains into refined blocks; (iii) transformation of the dense dislocation walls or cell walls into sub-boundaries; and (iv) evolution of sub-boundaries into conventional grain boundaries with large misorientations (or sharpening of grain boundaries).

* Corresponding author.
E-mail address: nrtao@imr.ac.cn (N.R. Tao).

1359-6454/$30.00
doi:10.1016/j.actamat.2006.07.013

As the dislocation cell size tends to a saturated value with continued plastic strain (e.g., ~100 nm for Cu [8,12]), a saturated grain size equivalent to the minimum cell size is expected with increasing strain. This has been observed in a number of materials processed by means of SPD techniques in which saturated grain sizes in the submicrometer regime have been obtained with increasing strain [13–15].

Experimental evidence has shown that extensive plastic deformation with high strain rates, such as ball-milling [16,17] and surface mechanical attrition treatment (SMAT) [10,18,19], may refine grains to the nanometer scale (5–30 nm), which is much smaller than that can be achieved with low strain rates (such as cold rolling, ECAP and HPT). The formation mechanism of nanosized grains induced by plastic straining is, in fact, not yet well understood. From an experimental point of view, the effect of high strain rates is obvious on formation of nanosized grains. Nevertheless, understanding the nanocrystallization mechanism following the dislocation processes as mentioned above is difficult. It is known that lattice dislocation activities (generation and pile-up) are effectively suppressed by extremely small grain dimensions. Formation of dislocation cells would not be feasible in nanosized grains. Two questions thus arise: What is the effect of strain rate on the grain refinement mechanism? And how are the nanosized crystallites formed during plastic deformation at high strain rates? The present work aims to answer these questions by a systematic examination of the microstructure evolution from macro to the nanometer scale with an increasing strain and strain rate in a pure Cu sample by using SMAT [20,21].

In the SMAT process described previously [10], a gradient variation of plastic strain and strain rate was achieved in the sample from the treated topmost surface to the deep matrix. The strain rate was estimated to be as high as 10^{2-3} s^{-1} (comparable to that of ball-milling) at the topmost surface, decreasing down to zero in the deep matrix (a few millimeters from the topmost surface). Consequently, a gradient microstructure is obtained descending through the sample, owing to different levels of strain rate and/or different degrees of plastic strain. This provides a unique opportunity to characterize the deformation mode of a material over a wide range of strain rate and to investigate the corresponding grain refinement mechanism by examining the microstructural features at different depths of a single treated sample. This methodology has been successfully applied to uncover the plastic strain-induced grain refinement mechanism in several material systems, including pure Fe [10], Ti [22], Al alloys [19], Ni alloys [23] and steels [24].

2. Experimental

A copper plate ($100 \times 100 \times 8$ mm^3) with a purity of 99.995 wt.% was subjected to SMAT. Before SMAT, the plate surface was polished with silicon carbide papers and annealed in vacuum at 973 K for 120 min to diminish the effect of mechanical processing and to obtain homogeneous coarse grains. The average grain size of the as-annealed sample is about 200 μm with a few annealing twins inside some grains.

The details of the SMAT set-up and processing have been described previously [10]. In brief, stainless steel balls were placed at the bottom of a cylinder-shaped vacuum chamber that was vibrated by a vibration generator, with which the balls were resonated to impact the sample surface. Because of the high vibration frequency, the entire surface of the treated sample was impacted with a large number of shots within a short period of time. In this work, samples were treated in vacuum at room temperature with stainless steel balls (8 mm diameter) at a vibration frequency of 50 Hz for 5 min (hereafter referred as to sample SMAT-5) and 30 min (sample SMAT-30), respectively. Microscopic observations and positron annihilation spectroscopy experiments confirmed that the surface layer of the SMAT samples is free of porosity or cracks.

The microstructural evolution of the SMAT Cu samples was characterized by using a JEM-2010 transmission electron microscope (TEM) operated at a voltage of 200 kV. Cross-sectional thin foils for TEM observations were prepared in the following steps: (i) electroplating a Ni layer of 1.5 mm thick onto the treated surface of the SMAT Cu samples; (ii) cutting a cross-sectional piece of the electroplated sample (with a diameter of 3 mm and a thickness of 0.5 mm) with the treated surface in the middle; (iii) grinding it carefully to about 30 μm thick; (iv) dimpling and ion thinning to perforation at room temperature.

The measurements of grain/cell sizes were made directly from TEM observations and the reported values are averaged from a few hundred grains (or cells) selected randomly. The misorientation angles between neighboring subgrains/grains were measured with the aid of a TEM double-tilt sample holder.

3. Results and discussion

Cross-sectional microstructures of the original and the SMAT Cu samples are shown in Fig. 1. Evidence of plastic deformation is obvious in the surface layer to a depth of about 300 μm for SMAT-5. The deformation is inhomogeneous in terms of depth from place to place, due to the varying orientations of grains and the heterogeneous nature of the plastic deformation within and between grains. After SMAT for 30 min, the deformation layer increased to a depth of about 800 μm, within which grain boundaries could hardly be identified. Compared to that in the SMAT pure Fe [10], 304 stainless steel [24] and low carbon steel samples [25], the deformation layer in the SMAT Cu sample is thicker under the same treatment conditions owing to its better plasticity and/or lower hardness.

Characterization of the SMAT samples at various depths by using cross-sectional TEM observations has been carried out to reveal the microstructural characteristics at

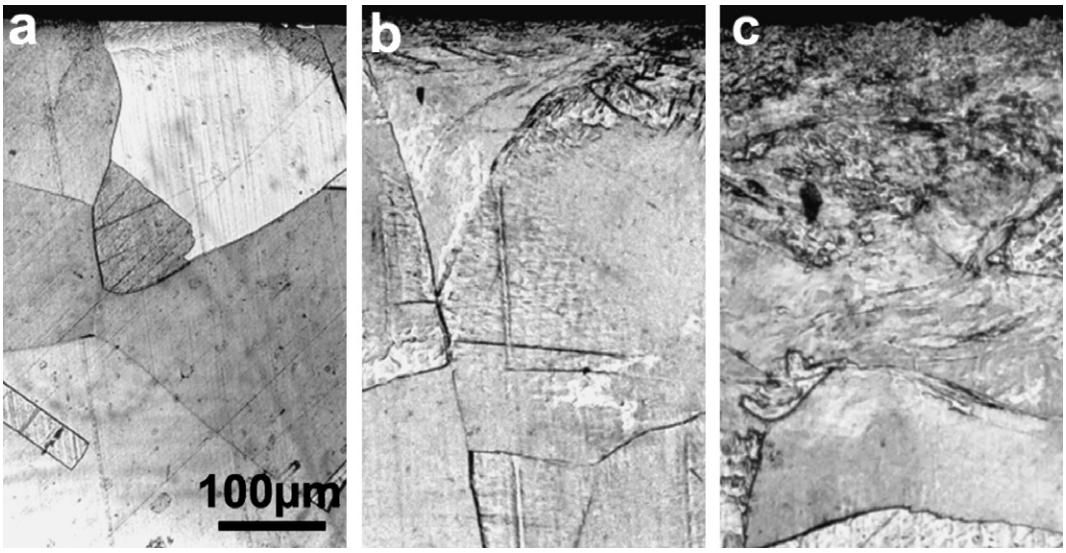

Fig. 1. Cross-sectional observations of the original (a), SMAT-5 (b) and SMAT-30 (c) samples.

different levels of strain and strain rate, and thereby to uncover the underlying grain refinement mechanism. Two different grain refinement mechanisms have been detected: in the deformation layer (>25 μm depth), grain refinement is primarily achieved via formation and evolution of dislocation cells (DCs), a process analogous to that observed in deformed coarse grains [8]; while in the top layer (<25 μm depth), mechanical twinning plays an important role in the grain refinement in both samples. In the following sections, grain refinement processes in the two subsequent layers will be described in detail.

3.1. Grain refinement via formation of dislocation cells (depth >25 μm)

3.1.1. SMAT-5 sample

Fig. 2 shows typical cross-sectional bright-field TEM images and corresponding selected area electron diffraction (SAED) patterns at different depths from the topmost surface (depth >25 μm) in SMAT-5. Adjacent to the strain-free matrix (Fig. 2(A1)), high-density dislocations are generated by plastic deformation and these are arrayed in tangles. At a depth of about 200 μm, DCs were formed inside the original grains (Fig. 2(A2)), which are roughly equiaxed (in three dimensions (3D)) with an average size of about 800 nm. From the corresponding SAED pattern (Fig. 2(B2)) it can be observed that the misorientations between the adjacent DCs are negligible. As the depth decreases, DC walls become thinner and the cell size reduces. At about 100 μm deep (Fig. 2(A3)), the average cell size drops to about 500 nm and the cell walls become much thinner than that in Fig. 2(A2). The corresponding SAED pattern (Fig. 2(B3)) shows small misorientations between the adjacent DCs.

Formation of DCs in deformed structures is driven by minimizing the total free energy of a high density of dislocations when the level of dislocation density increases to a certain value. Formation of equiaxal or elongated DCs in Cu during plastic deformation is commonly seen [8,12], and the sizes of these DCs are in the submicrometer range.

With a further decrease of depth, sharp sub-boundaries with substantial misorientations were observed occasionally (as in Fig. 2(A4) and (B4)). At a depth of 25 μm, the sizes of subgrains with sharp boundaries decreased to about 150 nm and misorientations between the subgrains are further increased (Fig. 2(A5) and (B5)). The majority of DCs and subgrains observed in this area are roughly equiaxed, though some elongated cells are occasionally observed. Because of the inhomogeneity of plastic deformation, some DCs and deformation twins inside original coarse grains are visible in this region; the latter will be described in detail in Section 3.2.1. It is noted that DCs with a size of <100 nm are seldom seen in TEM observations.

3.1.2. SMAT-30 sample

Compared to sample SMAT-5, SMAT-30 has a much thicker deformation layer. Above the deformation-free matrix, the deformation layer from about 800 to 200 μm deep is characterized by dislocation structures, which are arranged in DCs with sizes ranging from 1 μm to 200 nm. At a depth of 300 μm, well-developed DCs were formed (Fig. 3(A1)), in contrast to high-density dislocations in SMAT-5 at the same depth, across which obvious misorientations are noticed (Fig. 3(B1)). In the span from 200 to 25 μm, original grains were subdivided into submicro-sized grains and/or subgrains, most of which have roughly equiaxed shapes. As shown in Fig. 3(A2), most boundaries are sharply delineated and the contrast across them is small, i.e. these are typical images of sub-boundaries. The existence of subgrains with small misorientations is also

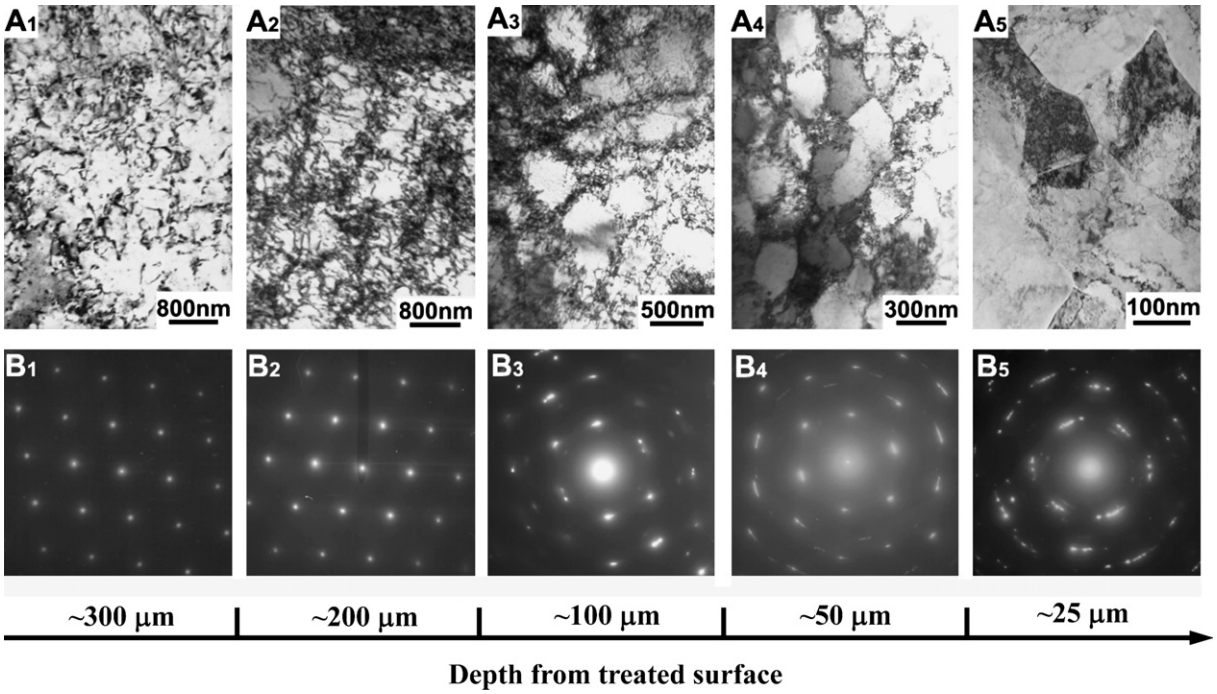

Fig. 2. Typical TEM images (A) and the corresponding SAED patterns (B) showing the microstructures at different depths (from 300 up to 25 μm, as indicated) from the topmost surface in SMAT-5 sample.

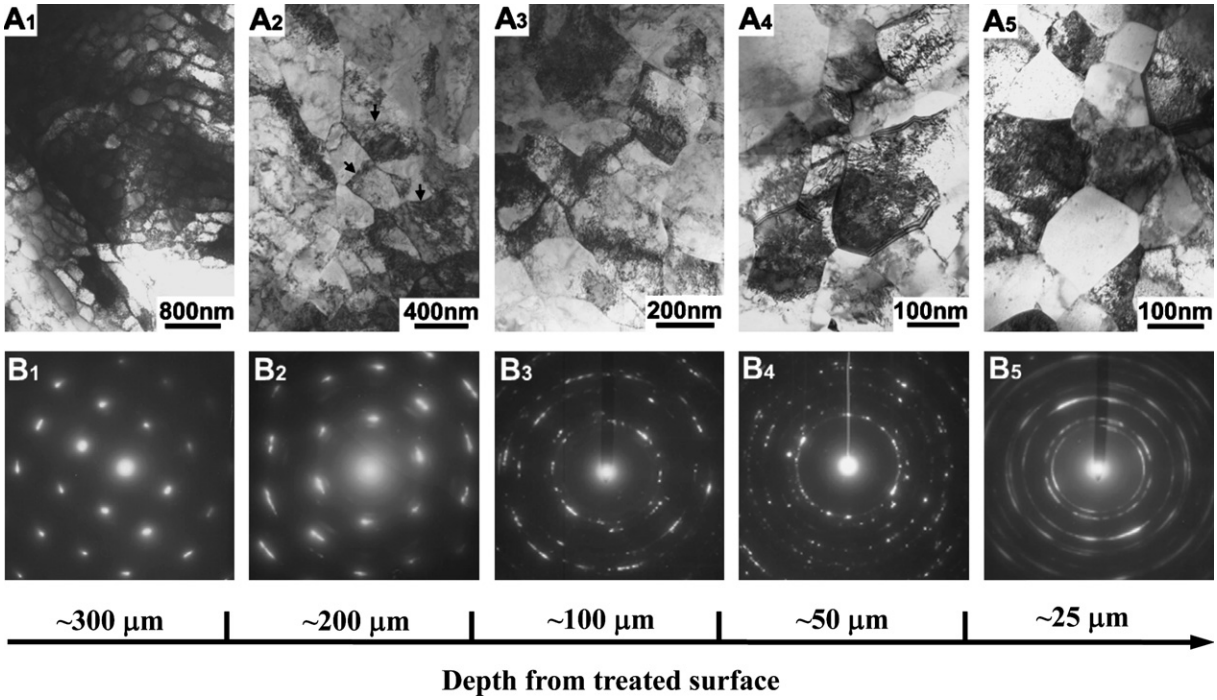

Fig. 3. Typical TEM images (A) and the corresponding SAED patterns (B) showing microstructures at different depths (from 300 up to 25 μm, as indicated) from the topmost surface in SMAT-30 sample.

confirmed by the corresponding SAED pattern (Fig. 3(B2)) in which scattered and elongated spots are shown. The misorientations across the neighboring subgrains are about a few degrees. It is noticed that some sub-boundaries have not yet been well developed from the DC walls, across which the misorientations are less than 1° (as indicated by solid arrows).

With decreasing depth, the subgrain/grain size decreases and the misorientation angle gradually increases, as shown in Fig. 3(A3) and (A4) and (B3, B4). Fig. 4(a) shows a

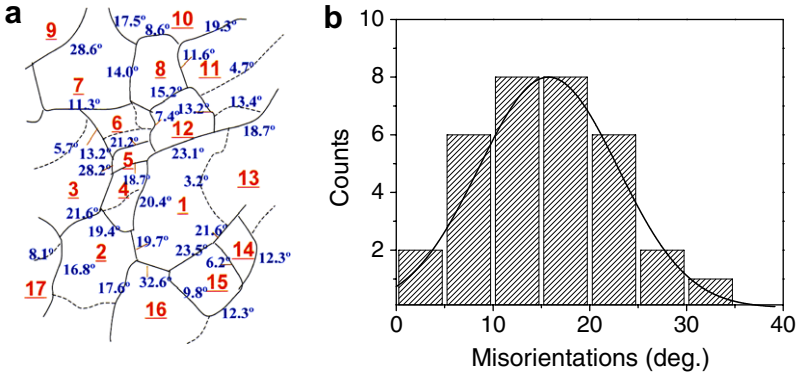

Fig. 4. Measured misorientations across adjacent refined grains in Fig. 3(A4) (a) and the corresponding statistical distribution of misorientations (b).

sketch of microstructure in Fig. 3(A4) with measured misorientation angles (marked with numbers) across grain boundaries. Most boundaries with distinct contrasts are found to be high-angle ones while sub-boundaries with low-angle misorientations exist inside some refined grains. The refined grains are further subdivided by the sub-boundaries. Low- to high-angle boundaries are spatially mixed throughout the microstructures due to the inhomogeneity of deformation, which is consistent with that in Cu after severe plastic deformation [8]. The misorientation angles distributed in a wide range from several to more than 30°, characterized by a normal logarithmic distribution (with an average value of 16°), as seen in Fig. 4(b).

At a depth of about 25 μm (Fig. 3(A5)), well-developed equiaxed grains sized about 100 nm are seen. The grain boundaries are clearly visible with an obvious contrast. The corresponding SAED pattern (Fig. 3(B5)) shows a set of rings without obvious preferential orientations, indicating the existence of highly misoriented grains. High-density dislocations are still present inside the grains, as is typical of microstructures developed by severe plastic deformation [3].

Based on the microstructure observations described above, a grain refinement mechanism via DCs in the SMAT Cu (depth $>\sim$25 μm) might be summarized as follows. The refinement involves the formation of DCs in original grains, transformation of cell walls into subgrain boundaries with small misorientations separating individual sub-grains, and evolution of sub-boundaries into highly misoriented grain boundaries (GB sharpening). This grain refinement process is continuous with increasing strain, in which dislocation activities dominate the process.

3.1.3. Variation of grain (or cell) size with depth (depth >25 μm)

From a large number of TEM images of both samples, the sizes of grains, subgrains and DCs were measured as a function of depth from the topmost treated surface, as plotted in Fig. 5. For SMAT-5, DCs were formed from depths of 200 up to 25 μm and a mixture of subgrains and grains was obtained in the 50–25 μm zone. For SMAT-30, DCs exist from depths of 800 to 200 μm, and refined grains and subgrains were observed in from 200 to 25 μm. For both samples, a decreasing trend is noticed for the grain/cell size with a reduction of depth, indicating that the grain refinement proceeds continuously with an increasing strain.

Compared to SMAT-5, the spans of both DCs and grains are much larger in SMAT-30. At the same depth, the sizes of DCs and grains in SMAT-30 are much less than those in SMAT-5, and the boundaries are better developed in SMAT-30. With a decrease in depth, the size difference between the two samples diminishes. At a depth of 25 μm, the average size of grains/DCs in SMAT-5 is about 160 nm, while the mean grain size in SMAT-30 is about 100 nm, as shown in Fig. 5(b). The grain size of about 100 nm is coincident with the steady-state size of refined grains when bulk Cu samples are processed by means of severe plastic deformation such as ECAP, HPT, repeated cold-rolling or multiple compressions [6,8,12].

In terms of the grain refinement mechanism, it is possible to locate the origin of the steady-state grain size induced by continuing plastic straining. It is known that formation of dislocation cells minimizes total strain energy. With an increasing plastic strain and a concurrent increase in dislocation density, DC size decreases. An empirical relationship between the cell size (d_{DC}) and the applied shear stress (τ) has been found [26]:

$$d_{DC} = \frac{KGb}{\tau} \tag{1}$$

where K is a constant with a value close to 10, G is the shear modulus and b is Burgers vector. This relation applies to the materials in which the applied shear stress is well in excess of the friction stress. It is apparent that with an increment of the applied shear stress, the cell size decreases, consistent with our experimental observations.

A limiting size of DCs can be estimated when a maximum shear stress is applied. Taking the maximum shear stress as $G/30$, a minimum cell size of $d^*_{DC} = 300b$ is obtained; hence, DCs may not be smaller in size than this value. In other words, formation of DCs smaller than

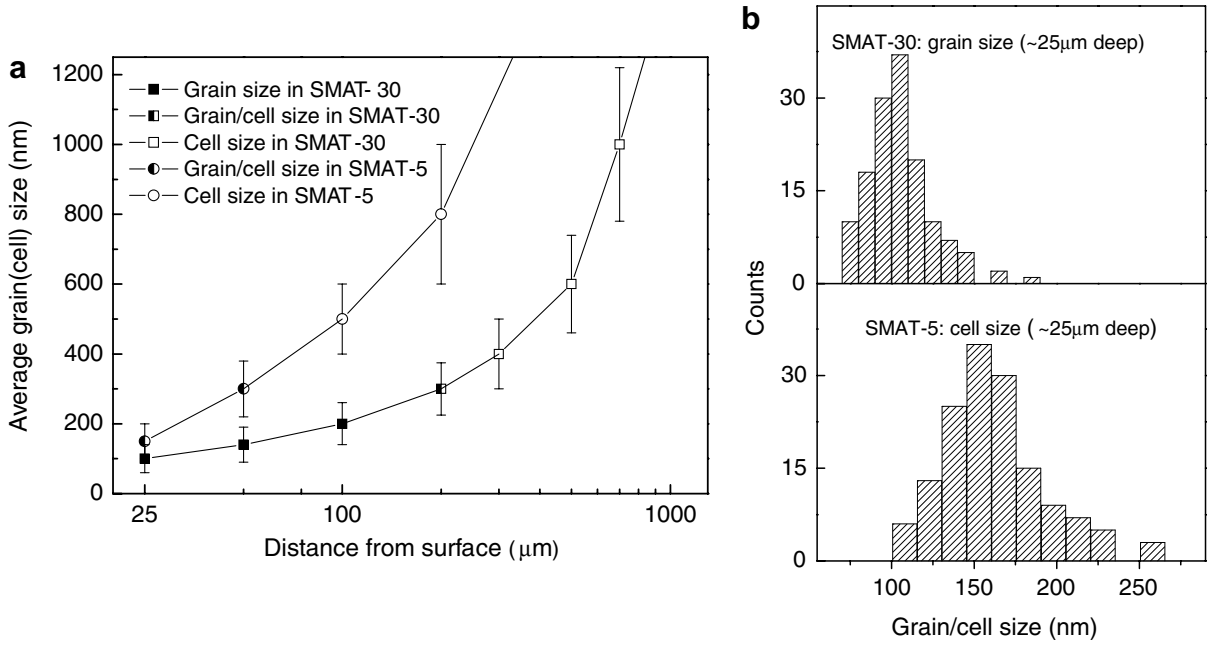

Fig. 5. Variation of grain/cell size with the depth from the topmost surface (>25 μm) (a) and statistic distributions of grain size and cell size at a depth of about 25 μm in two samples (b).

d^*_{DC} would require a shear stress even larger than the maximum shear stress, which is unrealistic. For Cu, d^*_{DC} is about 90 nm, which is consistent with the experimental observations reported in the literature. It was found that when drawing Cu wire the size of DCs decreases with an increasing drawing strain, tending to a saturation value of about 100 nm [27].

As discussed earlier, the eventual refined grains originate from the DCs formed in the early stage of plastic deformation. Therefore, the DC size limit will naturally be the limit of grain size obtainable via this grain refinement mechanism. The minimum grain size we obtained is about 100 nm in this deformation layer (thickness >25 μm) in the SMAT Cu samples, which agrees well with the predicted grain size limit (~90 nm).

3.2. Grain refinement via mechanical twinning (depth <25 μm)

3.2.1. SMAT-5 sample

Typical cross-sectional TEM images at different depths in the top surface layer (depth <~25 μm) of sample SMAT-5 are shown in Fig. 6, in which multiple mechanical twins within coarse grains are evident. The mechanical twin density (or the twin/matrix lamella thickness) varies from grain to grain due to different crystallographic orientations of the grains. From a large number of TEM observations, we noticed a general trend that with a decrease of depth, the twin density increases substantially. In the top layer, thicknesses of both twin and matrix are remarkably refined, down to as small as a few nanometers (as shown in Fig. 6(c)).

The lengths of twins are about several hundred nanometers. Within a coarse grain, multiple twins are formed, which may initiate from stress concentrations at grain boundaries or junctions. Unlike SMAT 304 stainless steel [24], no twin–twin intersection was found in the present sample. Apparently, formation of these high-density nano-sized twins introduced a large number of twin boundaries (TBs) subdividing the original coarse grains into lamellar nanocrystallites with special crystallographic orientations.

A close observation of the nano-sized mechanical twins is shown in Fig. 7. The corresponding SAED pattern shows a superposition of two $\langle 0\,1\,1\rangle$ diffraction patterns which are symmetrical to each other with respect to the $\{1\,1\,1\}$ plane, indicating that the lamellar structure observed consists of alternate stacks of twins and matrix. Therefore, we referred as this structure to twin–matrix (T–M) lamellae. Fig. 7(c) is a high-resolution electron microscope (HREM) image of the outlined region in Fig. 7(a), which shows clearly the T–M lamellar structure. Dislocations and steps are seen at TBs, and are typical characteristics of mechanical twins, in contrast to annealing twins or growth twins in which the TBs are almost dislocation-free [28].

Dislocations are observed inside twins and matrix as well, but dislocation cell structures could not be identified in this regime. Dislocation arrays or walls are formed inside some T–M lamellae, as seen in Fig. 8. The dislocation walls are perpendicular to the TBs with a spacing of several tens of nanometers. At the intersection of TBs and dislocation walls, an obvious change in orientation of the TB is identified. Therefore, the TBs become curved.

Formation of multiple twins is quite common in the deformation process of materials with medium to low

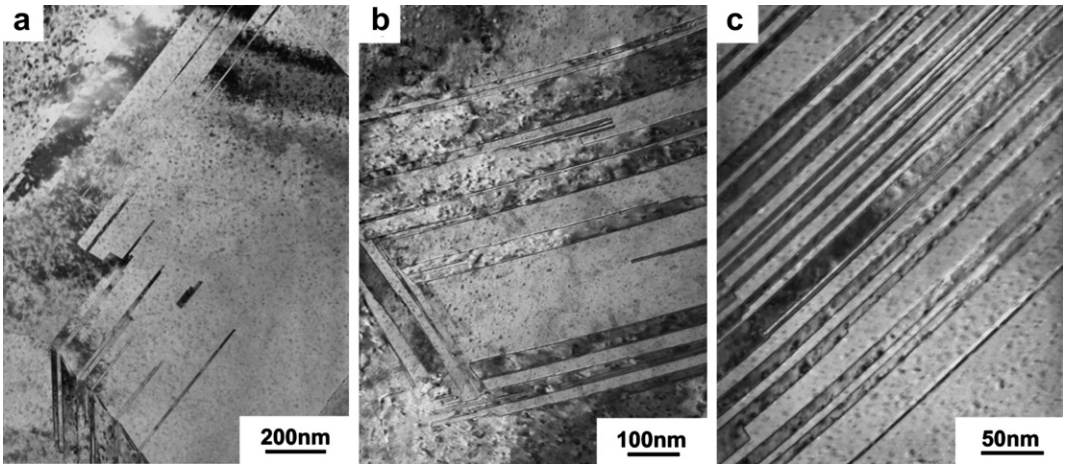

Fig. 6. Typical TEM images showing T–M lamella structures at different depths from the topmost surface in SMAT-5 sample: (a) 25 μm deep, (b) 10 μm deep and (c) the very top surface.

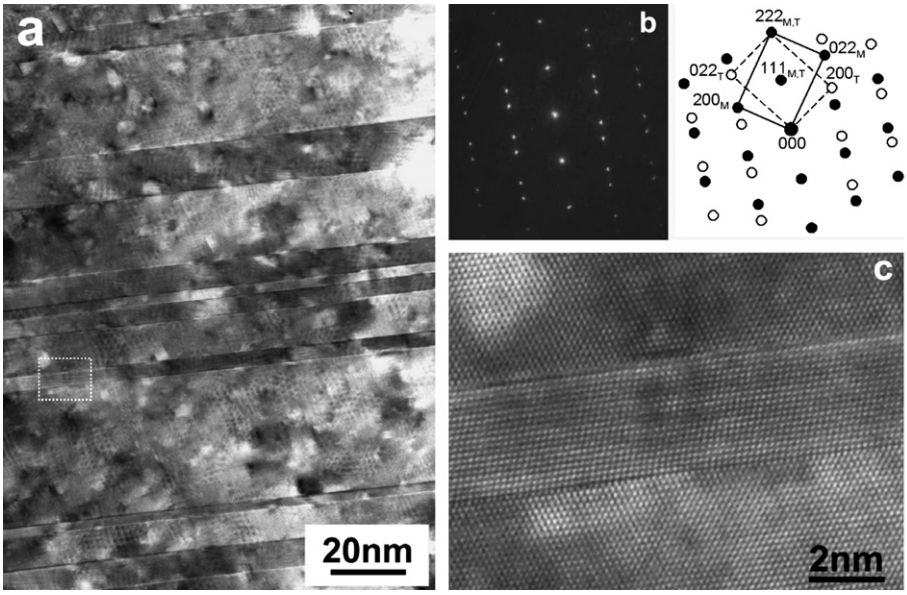

Fig. 7. HREM images (a and c) and a corresponding SAED pattern (b) of the T–M lamella structure in the top surface layer of SMAT-5 sample.

SFEs, especially at high strain rates and/or low temperatures as dislocation slips are effectively suppressed. In face-centred cubic (fcc) metals, the tendency to substitute twinning for slip is more sensitive to the strain rate [29]. For example, nanosized thick mechanical twins are frequently formed in the Cu samples processed by shock-loading [30], ball milling [16] and dynamic plastic deformation [31]. During the SMAT process, the topmost surface layer is deformed at high strain rates (estimated to be as high as 10^2–10^3 s^{-1}), hence twinning would be effectively activated and numerous nanosized thick twins formed in the top surface layer.

3.2.2. SMAT-30 sample

In the 0–25 μm thick surface layer in sample SMAT-30, average grain sizes are found to decrease gradually from about 100 nm (at ~25 μm deep) to about 10 nm (topmost layer).

In the layer close to ~25 μm deep, high-density dislocations are observed in the submicron-sized grains, and multiple mechanical twins appeared inside many grains of about 100 nm or less in size, as shown in Fig. 9. In each grain, twin boundaries are parallel to each other and they subdivide the grain into a thin T–M lamellar structure, of which the thickness varies from several to several tens of nanometers. The lengths of the twins, about 100 nm or less, are comparable to the grain size. Dislocations are still visible in the lamellar nanostructures.

More twins were observed with a decrease of thickness owing to an increased strain rate and plastic strain. It is interesting to note that inside the T–M lamellae, high-density dislocations exist and the two-dimensional (2D)

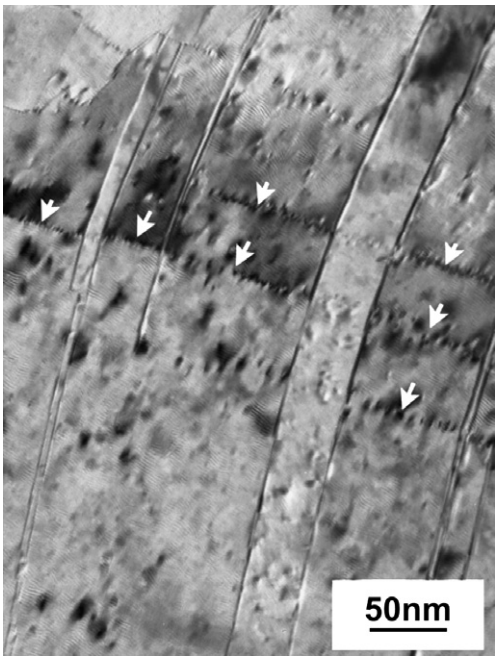

Fig. 8. A TEM image showing dislocation arrays (as indicated by arrows) in the T–M lamellae in SMAT-5 sample (close to the topmost surface).

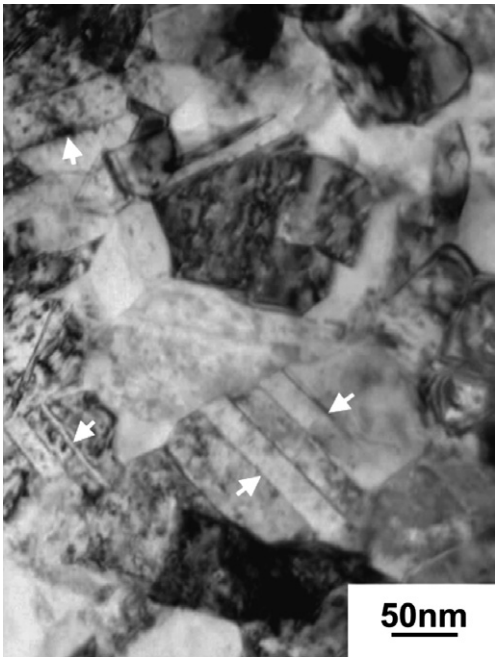

Fig. 9. A typical TEM image showing formation of multiple twins inside various refined (submicron-sized) grains at a depth of about 20 μm in SMAT-30 sample.

lamellae are further refined by dislocation arrays or walls. As shown in Fig. 10, several dislocation walls (as marked with arrows), roughly perpendicular to the twin boundaries, are formed in the lamellae. This scenic was very likely developed from dislocation arrays (as seen in Fig. 8) by accumulating more dislocations in the lamellae. The spacing between dislocation walls varies from lamella to lamella, and is several tens of nanometers. These dislocation walls are eventually developed into sub-boundaries and boundaries accompanied by increasing misorientations, dividing the 2D lamellae into 3D equiaxed nanosized structures. High-density dislocations were still observable inside about 50 nm grains.

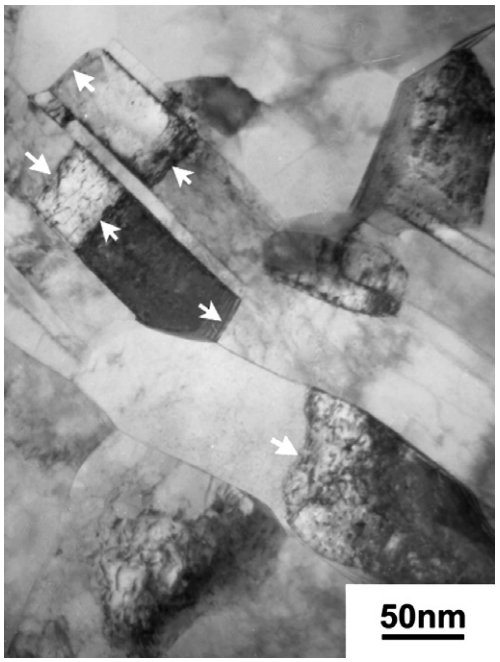

Fig. 10. A TEM image showing formation of dislocation walls (as indicated by arrows) inside twin lamellae in SMAT-30 sample.

Formation of randomly orientated nanosized grains from "cutting" 2D T–M lamellae by perpendicular dislocation walls can also be evidenced by a close analysis of the orientation relationship between adjacent grains. Fig. 11(a) and (b) shows typical bright- and dark-field TEM images of nanostructures in the top surface layer. From the images, one can see that roughly equiaxed nanocrystallites were formed and they seem to be arranged in parallel arrays in feature. The corresponding SAED pattern from a large area (Fig. 11(c)) showed elongated spots, indicative of rather large misorientations (roughly random). However, the nanobeam diffraction (NBD) pattern (Fig. 11(d)) of some adjacent grains indicated fcc twin relations between them. This indicated clearly that in a relatively large area with many nanograins, random orientations are seen, while the neighbouring nanograins still remain, to some extent, preferential orientations of original T–M lamellae. This finding provides a strong evidence to support the argument that the nanocrystallites originate from "cutting" nanometer-thick T–M lamellae by dislocation activities.

Equiaxed nanocrystallites with random orientations were observed close to the top surface. Fig. 12 shows a typical TEM image from a depth of several micrometers. The microstructure is characterized by nanometer-sized, equiaxed grains. The corresponding SAED pattern (identified

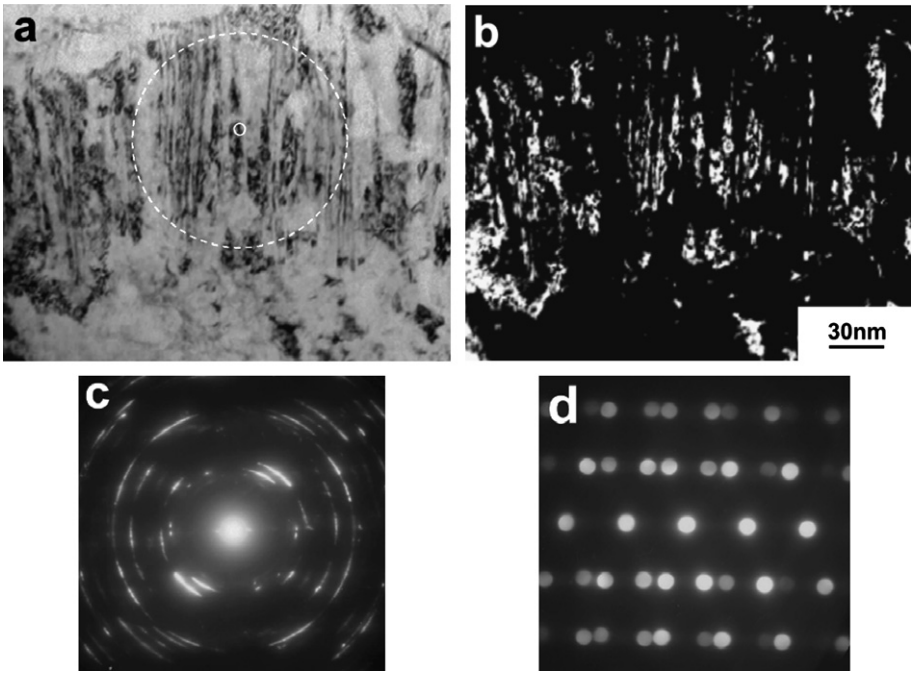

Fig. 11. TEM observations of the microstructure very close to the topmost surface in SMAT-30 sample showing nanocrystallites derived from T–M structures: (a) bright-field image, (b) dark-field image, (c) a SAED corresponding to the large circle in (a), and (d) the micro-area electron diffraction pattern corresponding to the small circle in (a).

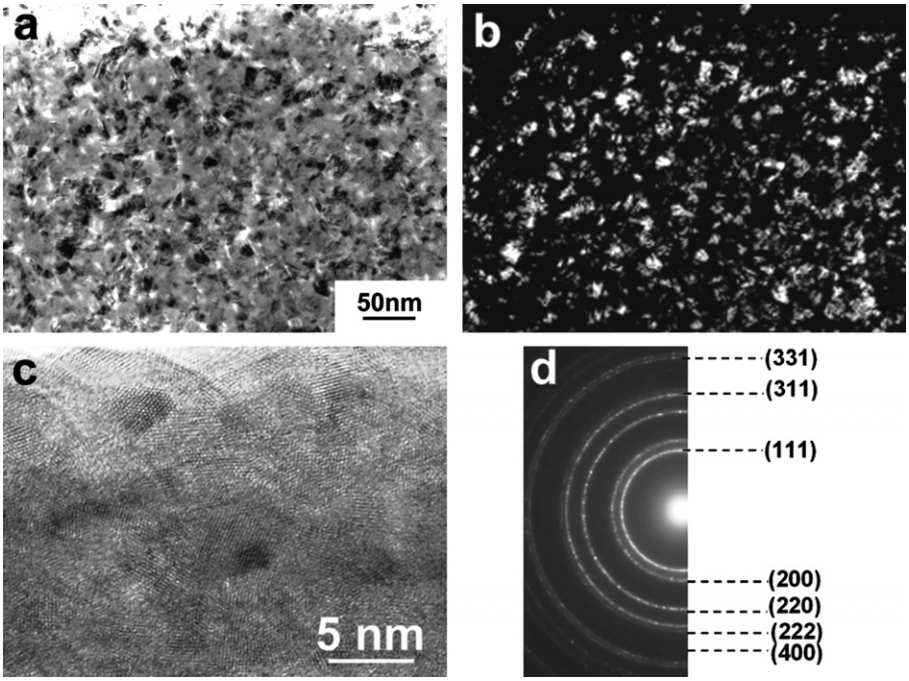

Fig. 12. (a) Bright-field image, (b) dark-field image, (c) HREM images and (d) the corresponding SAED of the topmost surface layer structure in SMAT-30 sample.

as fcc polycrystalline Cu) shows fairly uniform rings, indicating a continuous and wide distribution of misorientations among the nanograins. The average grain size obtained from the dark-field images is about 10 nm. A close observation of the nanostructure in the top surface layer was also performed under HREM, as shown in Fig. 12(c). The nanosized crystallites with different misorientations could be clearly identified.

It should be noted that in the topmost layer of a few micrometers thick, some of the contaminations introduced during the SMAT processing (such as iron and oxygen) could not be excluded, although no other phase has been

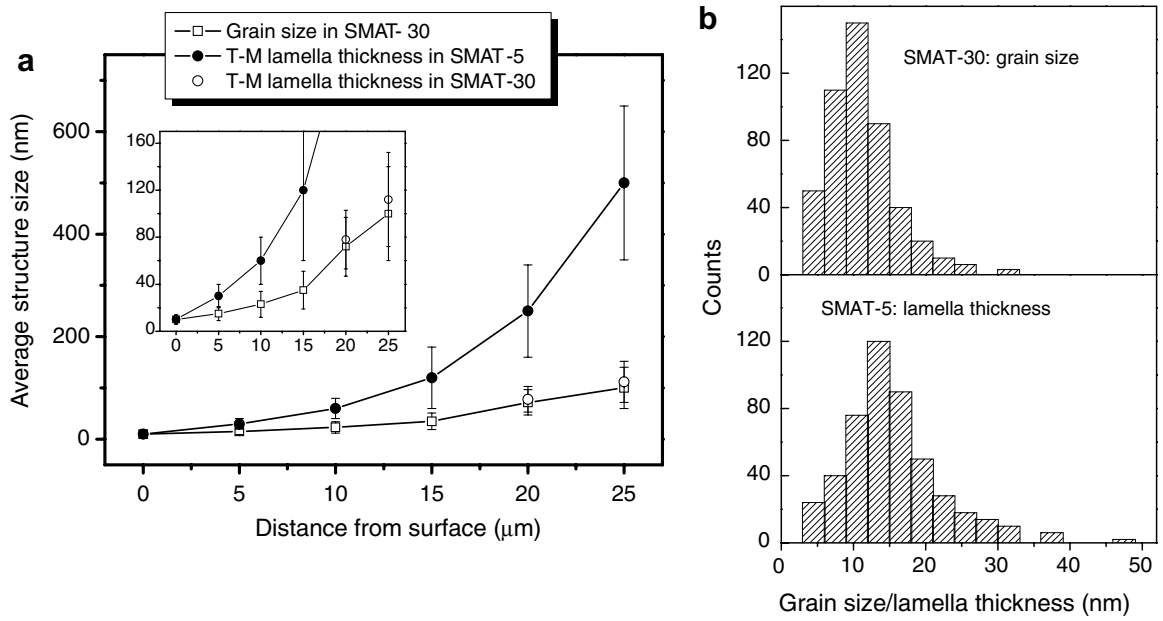

Fig. 13. Variation of grain/cell size with the depth (<~25 μm) from the topmost surface (a) and statistical distributions of grain size and T–M lamella thickness in the top surface layer in two samples (b).

identified from the electron diffraction except pure fcc Cu. The extremely fine grains (~10 nm) might be stabilized by the contaminations.

Unlike the grain refinement process via DCs in the subsurface layer, twinning plays an important role in grain refinement in the top surface layer at high strain rates. High-density mechanical twins induce numerous TBs to subdivide the original grains into special oriented lamellar nanostructures. Strain-induced dislocation walls further subdivide lamellar nanostructures into equiaxed nanostructures. Apparently, the boundaries of these equiaxed structures consist of twin boundaries and dislocation boundaries. As numerous dislocations accumulate and annihilate at these boundaries, they developed into randomly oriented, large-angle boundaries. Such a grain refinement process involving the interactions of strain-induced twins and dislocations has been found in the SMAT Ni-based alloy [23,32]. The average size of obtained grains is obviously dependent upon the thickness of T–M lamellae. When deformed at high strains and strain rates, the thickness of T–M lamellae is as small as several nanometers, as seen in Fig. 7. For deformed Cu, the average size of grains refined via mechanical twins is usually in the nanometer range, i.e. much smaller than the size of grains refined via DCs (submicrometer scale).

3.2.3. Variations of grain size and T–M lamellae thickness with depth (<25 μm)

The average grain sizes and T–M lamella thickness determined from TEM observations as a function of depth (<25 μm) in SMAT-5 and SMAT-30 samples are summarized in Fig. 13. For SMAT-5, mechanical twins were formed in the range of 0–25 μm deep and the average thickness of T–M lamellae decreased from a few hundred to several nanometers with decreasing depth. The average lamella thickness tends to about 10 nm in the top surface (as shown in Fig. 13(b)).

In SMAT-30, mixtures of nanosized grains and nanometer-thick T–M lamellae were obtained in the region of from 25 up to 20 μm deep. In the top layer with depth <15 μm, only equiaxed nanograins were detected. Both the T–M lamella thickness and the grain size decrease gradually with a reduction of depth. The average size of nanocrystallites in the top surface is about 10 nm for the SMAT-30 sample, as indicated in Fig. 13(b).

It is interesting to note that the minimum T–M lamellar thickness in SMAT-5 is comparable to the minimum grain size in SMAT-30 in the very top surface layer, both being about 10 nm. This coincidence provides further evidence to support the proposed refinement mechanism that the equiaxed nanocrystallites result from the "cutting" of nanometer-thick T–M lamellae by dislocation activities.

4. Conclusions

Plastic strain-induced grain refinement in Cu closely relates to its deformation modes. In the SMAT Cu samples studied, we identified two different strain-induced grain refinement mechanisms corresponding to different levels of strain rate.

In the subsurface layer (thickness >25 μm) of the SMAT Cu samples, where strain rate is low and the plastic deformation is dominated by dislocation activities, submicron-sized grains were obtained via formation and development of dislocation cells. The minimum size of the refined grain is approximately 100 nm. The grain refinement process

involves formation of DCs in original grains, transformation of DC walls into sub-boundaries with small misorientations separating the initial grains into individual subgrains, and evolution of sub-boundaries into highly misoriented grain boundaries.

In the top surface layer (thickness $<25\ \mu m$) of the SMAT Cu samples, strain rates are much elevated so that deformation twinning plays an important role in plastic deformation. The grain refinement process includes: (i) formation of high-density, nanometer-thick twins dividing the original coarse grains into T–M lamellae; (ii) development of dislocation walls that further subdivide the T–M lamellae into equiaxed nanosized blocks; and (iii) evolution of these preferentially oriented blocks into randomly oriented nanosized grains. The minimum size of refined grains is about 10 nm.

This study clearly demonstrates that strain rate plays a critical role in the plastic strain-induced grain refinement processes and in the minimum grain size obtainable via plastic deformation.

Acknowledgements

Financial support from the National Natural Science Foundation of China (Grants Nos. 50021101, 50431010 and 50071061) and the Ministry of Science and Technology of China is acknowledged.

References

[1] Hansen N. Metall Mater Trans A 2001;32:2917.
[2] Ueji R, Tsuji N, Minamino Y, Koizumi Y. Acta Mater 2002;50:4177.
[3] Valiev RZ, Islamgaliev RK, Alexandrov IV. Prog Mater Sci 2000;45:103.
[4] Iwahashi Y, Horita Z, Nemoto M, Langdon TG. Acta Mater 1998;46:3317.
[5] Lowe TC, Zhu YT. Adv Eng Mater 2003;5(5):373.
[6] Hebesberger T, Stüwe HP, Vorhauer A, Wetscher F, Pippan R. Acta Mater 2005;53:393.
[7] Wang YM, Chen MW, Sheng HW, Ma E. J Mater Res 2002;17:3004.
[8] Belyakov A, Sakai T, Miura H, Tsuzaki K. Philos Mag A 2001;81:2629.
[9] Bay B, Hansen N, Hughes DA, Kuhlmann-Wilsdorf D. Acta Metall Mater 1992;40:205.
[10] Tao NR, Wang ZB, Tong WP, Sui ML, Lu J, Lu K. Acta Mater 2002;50:4603.
[11] Mishra A, Richard V, Grégori F, Asaro RJ, Meyers MA. Mater Sci Eng A 2005;410–411:290.
[12] Torre FD, Lapovok R, Sandlin J, Thomson PF, Davies CHJ, Pereloma EV. Acta Mater 2004;52:4819.
[13] Hughes DA, Hansen N. Phys Rev Lett 2001;87:135503-1.
[14] Shin DH, Kim I, Kim J, Park K. Acta Mater 2001;49:1285.
[15] Gholinia A, Prangnell PB, Markushev PB. Acta Mater 2000;48:1115.
[16] Huang JY, Wu YK, Ye HQ. Acta Mater 1996;44:1211.
[17] Mohamed FA, Xun Y. Mater Sci Eng A 2003;354:133.
[18] Tao NR, Sui ML, Lu J, Lu K. Nanostru Mater 1999;11:433.
[19] Wu X, Tao N, Hong Y, Xu B, Lu J, Lu K. Acta Mater 2002;50:2075.
[20] Lu K, Lu J. J Mater Sci Technol 1999;15:193.
[21] Lu K, Lu J. Marer Sci Eng A 2004;60:891.
[22] Zhu KY, Vassel A, Brisset F, Lu K, Lu J. Acta Mater 2004;52:4101.
[23] Tao NR, Wu XL, Sui ML, Lu J, Lu K. J Mater Res 2004;19:1623.
[24] Zhang HW, Hei ZK, Liu G, Lu J, Lu K. Acta Mater 2003;51:1871.
[25] Wang ZB, Lu J, Lu K. Acta Mater 2005;53:2081.
[26] Courtney TH. Mechanical behavior of materials. 2nd ed. New York (NY): McGraw-Hill; 1990.
[27] Embury JD. In: Kelly A, Nicholson RB, editors. Strengthening mechanisms in crystals. New York (NY): Wiley; 1971. p. 331.
[28] Lu L, Shen YF, Chen XH, Qian LH, Lu K. Science 2004;304:422.
[29] Christian JW, Mahajan S. Prog Mater Sci 1995;39:1.
[30] Murr LE, Niou CS, Garcia EP, Ferreyra E, Rivas JM, Sanchez JC. Mater Sci Eng A 1997;222:118.
[31] Zhao WS, Tao NR, Guo JY, Lu QH, Lu K. Scripta Mater 2005;53:745.
[32] Tao NR, Zhang HW, Lu J, Lu K. Mater Trans 2003;44:1919.